Sensors and Materials, Vol. 35, No. 6 (2023) 1995–2011
MYU Tokyo

S & M 3303

UV-curable Polydimethylsiloxane Photolithography and Its Application to Flexible Mechanical Metamaterials

Ten Sekiguchi,[1] Hidetaka Ueno,[2] Vivek Anand Menon,[3] Ryo Ichige,[1] Yuya Tanaka,[1] Hiroshi Toshiyoshi,[3] and Takaaki Suzuki[1*]

[1]Gunma University, 1-5-1 Tenjin-cho, Kiryu, Gunma 376-8515, Japan
[2]Kobe University, 1-5-1 Minatojima-minamimachi, Chuo-ku, Kobe, Hyogo 650-0047, Japan
[3]The University of Tokyo, 4-6-1 Komaba, Meguro-ku, Tokyo 135-8505, Japan

(Received February 13, 2023; accepted June 19, 2023)

Keywords: UV-PDMS, photolithography, polydimethylsiloxane, mechanical metamaterial, backside exposure

Polymers are increasingly being used as flexible structural materials in MEMS. We have focused on UV-cured polydimethylsiloxane (UV-PDMS), which is both photoreactive and highly flexible. In this study, we propose a photolithography-based patterning method to enable the microfabrication of UV-PDMS. The processing conditions related to patterning accuracy were also investigated. Furthermore, as a demonstration of the practical advantages of this processing method, free-standing flexible metamaterials with a negative Poisson's ratio were fabricated and uniaxial tensile tests were performed. The results showed a minimum Poisson's ratio of −1.30. Compared with the same type of specimen fabricated with a common permanent structural photoresist, the UV-PDMS specimen exhibited deformation approximately 12 times larger.

1. Introduction

With the recent development in the MEMS field, polymers have attracted attention owing to the low extensibility of conventional materials such as glass, silicon, and metals, which is around 0.1%, as well as their chemical and environmental impact.(1) Polymers have a very high affinity for soft MEMS(2) owing to their excellent material properties such as low Young's modulus, large deformation potential, and high strength. In addition, MEMS often requires approximately 100-μm-thick films,(3) and thick polymer layers can be easily deposited in the liquid phase with subsequent curing. By taking advantage of the above material properties, various devices have been fabricated and continue to be developed using polymer materials.(4,5) Furthermore, an increasing variety of existing polymer materials are being applied to MEMS, and new polymers are constantly being developed.(6–9) Among these, SU-8 thick-film photoresists for permanent structures and thermoset polydimethylsiloxane (PDMS) are the current mainstays of polymer-based microfabrication. They are used in various devices owing to their ability to form structures with high aspect ratios and high biocompatibilities. However, SU-8 is relatively inflexible,

*Corresponding author: e-mail: suzuki.taka@gunma-u.ac.jp
https://doi.org/10.18494/SAM4351

ISSN 0914-4935
https://myukk.org/

whereas PDMS has disadvantages such as thermal shrinkage and deformation as well as the need for casting molds to fabricate structures.

Regarding these issues of the polymer materials for MEMS, we have focused on UV-PDMS, a photocurable silicone rubber that can be cured by UV irradiation and is also highly flexible. UV-PDMS, a material not for patterning purposes originally, was previously investigated in the field of MEMS, for example, in the molding of microfluidic channels[10] and patterning by direct writing.[11] In these processes, molding cannot usually prevent the formation of a base plate covering during mold pouring, making it difficult to form a through-structure, and the processing area is limited in direct writing. It can be expected, therefore, that batch photopatterning at the wafer level via photolithography would improve the applicability of UV-PDMS in a wide range of soft MEMS.

In this study, a patterning method using photolithography is proposed as a wafer-level microfabrication method for UV-PDMS to form a flexible through-microstructure, which is difficult with the conventional molding process and the conventional thermally cured PDMS. The processing conditions were investigated with respect to spin film thickness, exposure dose, post-exposure baking, and development as factors affecting the patterning accuracy. Mechanical metamaterials (MMs) with a negative Poisson's ratio were also fabricated as a demonstration of the technique: tensile specimens of UV-PDMS and conventional thick photoresist for permanent structures were prepared and compared in terms of Poisson's ratio and strain rate. In this way, the use of photolithographically patterned UV-PDMS was verified as a practical solution for application in soft MEMS.

2. Microfabrication Principle for UV-PDMS

2.1 Photocurable silicon rubber UV-PDMS

A UV-curable liquid silicone rubber is a material that can be cured by exposure to UV radiation and is widely used as an adhesive pad for laminating touch panels such as car navigation systems, fixing precision components, and transporting ultrafine electronic components. In the MEMS field, it is being considered as a material for device structures produced by UV molding and UV nanoimprinting, as well as an adhesive material for microcomponents.

The UV-PDMS used in this study (KER-4690-A/B, Shin-Etsu Chemical Co., Ltd) is cured via the reaction shown in Fig. 1 by mixing KER-4690-A and KER-4690-B in a 1:1 ratio.[12] The viscosity of the liquid form after mixing is 3 Pa·s. Such UV-PDMS is fully cured by UV exposure at a dose of 3000 mJ/cm^2 in the liquid phase and being allowed to rest at 23 °C for 24 h. The solubility parameter (SP value), which represents the affinity between the precursor materials, is 7.4. The mechanical properties of UV-PDMS are comparable to those of the more conventional thermally cured PDMS with a tensile strength of 7.9 MPa, an elongation at fracture of 110%, and a Young's modulus of about 3 MPa. Critically, UV-PDMS and conventional PDMS are more elastic than conventional thick-film photoresists such as SU-8 when used as a MEMS structural material.

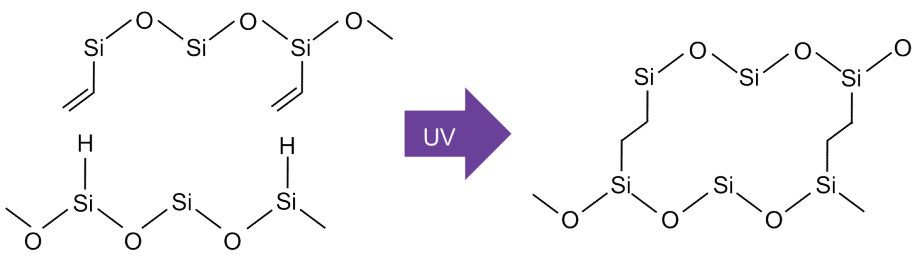

Fig. 1. (Color online) Chemical mechanism of UV-PDMS curing. A hydrosilylation reaction under a photoactivated catalyst cures vinyl and hydrosilyl silicone polymers.

2.2 Patterning principle based on photolithography

In this study, backside UV exposure is used as the patterning method for UV-PDMS. The backside exposure method is often used owing to the variety of achievable fabrication geometries, such as conical structures,[13] microlens arrays using diffraction,[14] and hollow metal microneedle arrays.[15] In contrast, we use the backside exposure method owing to the specific curing mechanism of UV-PDMS in this study.

UV-PDMS must be UV-exposed in a fully liquid state and then cured at room temperature. This means that it is not possible to immobilize the coated film on the substrate via soft baking prior to exposure as with conventional photoresists. Additionally, the coated film cannot be in direct contact with a photomask as usually required in frontside lithography since film uniformity would be compromised. Therefore, as shown in Fig. 2, UV-PDMS is deposited onto a transparent substrate featuring a light-shielding metal pattern, the substrate is held horizontally with the liquid deposition surface facing vertically upward, and the UV-PDMS in solution is exposed from the bottom through the underside of the transparent substrate.

2.3 Fabrication process

The process is divided into a mask-copying step to transfer the light-shielding pattern onto a glass substrate and a UV-PDMS backside exposure step using the substrate. A 30 mm × 40 mm × 550 μm glass substrate (CS00553, Matsunami Glass Ind., Ltd.) was used as the handle substrate during processing. An Al film was deposited on the surface of the cleaned glass substrate using a vacuum thermal evaporation system (VPC-1100, ULVAC) to provide a light-shielding film of approximately 200 nm thickness. Al was then patterned using positive photoresist S1813 (MICROPOSIT S1813G, Rohm and Haas Electronic Materials K.K.) and mixed acid P solution (Morita Chemical Industries Co.). The remaining S1813 was then removed with a remover (MICROPOSIT REMOVER 1165, Rohm and Haas Electronic Materials K.K.) to form a metal mask pattern on the glass substrate.

Liquid UV-PDMS was then spin-coated onto the Al-patterned glass substrate. After deposition, liquid UV-PDMS was exposed from the backside of the glass substrate without a

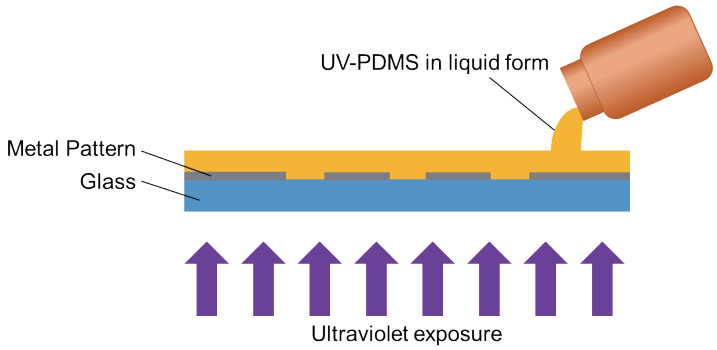

Fig. 2. (Color online) Schematic of backside exposure for liquid UV-PDMS. A light-shielding pattern is first formed on a glass substrate with a thin metal film. Liquid UV-PDMS is spin-deposited onto the pattern and exposed from the back of the substrate, keeping the stage horizontal to prevent the UV-PDMS from flowing down.

general photoresist soft bake. A post-exposure bake (PEB) was then performed and the unexposed areas were dissolved and removed using a solvent development process forming the final structure. The UV-PDMS film can be easily peeled off the glass substrate as a single film without the need for any release material or sacrificial layer release process.

3. Evaluation Methods

Various processing parameters were investigated to assess the viability of the fabrication process and resulting structure. The processing characteristics evaluated included thickness control through spin coating conditions and pattern accuracy through exposure, bake, and development conditions.

3.1 Thickness control

The effects of viscosity and spin coating speed on the resulting UV-PDMS sample thickness were evaluated by comparing samples under the following conditions. UV-PDMS was deposited using a spin coater (1H-DX2, Mikasa Corp.) in the same way as for resist coating in general photolithography, and half of the sample was UV-exposed at a dose of 3000 mJ/cm^2 by using a deep UV lamp (Optical ModuleX SX-UID501MAMQQ, USHIO INC.), a light source capable of general vertical exposure of thick-film photoresist. The sample was then baked at 100 °C for 3 min and developed, after which the resulting surface was evaluated. The film thickness at the step was measured using a surface roughness meter (surfcom 130A, Tokyo Seimitsu Co., Ltd.). Two types of liquid UV-PDMS were prepared: one with normal viscosity and one with reduced viscosity by toluene dilution. The initial viscosity of UV-PDMS was measured using a viscometer (DV-II+Pro, Brookfield). That of the normal UV-PDMS was 3 Pa·s, the same as the catalogue value, and that of the diluted UV-PDMS was 485 mPa·s. Spin coating speeds were 1000, 2000, 3000, and 4000 rpm. A spin curve was constructed by calculating the mean and standard deviation from measurements at several locations on each sample, and its controllability was verified from the relationship between spin speed and film thickness.

3.2 Patterning accuracy

The patterning accuracy of UV-PDMS was evaluated by measuring the test patterns processed by the proposed method. Two mask patterns with lines and spaces of 100:100 and 50:150 (μm) were used as the test patterns to be produced, and their lengths were measured using a scanning electron microscope (SEM; JCM-5700LV, JEOL). The exposure dose, PEB temperature, and solvent SP value used for development, which are related to patterning accuracy, were evaluated as the variable process conditions and are shown in Table 1.

The pattern widths at the top, middle, and bottom of the line structures were measured three-dimensionally as viewed from the top of the pattern. The widths were calculated using luminance profile analysis in ImageJ (NIH) image analysis software. The luminance values in the direction of the line width were obtained from the SEM image. From the obtained luminance profile, three characteristic line widths were evaluated across the center of the convex line profile as shown in Fig. 3: (i) the interval between the lowest luminance position on the outside of each convex

Table 1
Process conditions used to evaluate pattern accuracy. Samples were prepared using the parameters listed in bold as the default values. When otherwise not specified, the default values were used.

Exposure dose (mJ/cm^2)	800	1000	**1500**	2000	2500	3000
PEB temperature (°C)	23	75	**100**		150	200
Time	24 h	3 min	**3 min**		3 min	3 min
Solubility parameter	7.3	9.1		**9.8**		10.0
(Solvent)	(Hexane)	(Tetrahydrofuran)		**(Toluene)**		(Acetone)

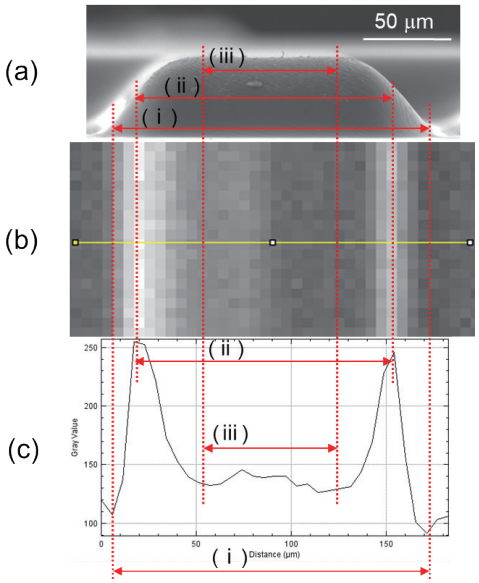

Fig. 3. (Color online) Method of obtaining luminance profiles from SEM images of a 100 μm nominal width pattern. (a) Cross-sectional SEM view of a line pattern. The microstructures were exposed from the bottom of the image. Note the convex sloped profile. (b) Top SEM view of the line pattern. The yellow line indicates the profile across which evaluation is performed. (c) Luminance profile across the line in (b). The red dotted lines indicate the structure lower width (i), middle width (ii), and upper width (iii). The middle width was chosen to evaluate against the nominal line width.

(structure lower width), (ii) the interval between the highest luminance position on the inside (structure middle width), and (iii) the interval between the lowest luminance position on the inside (structure upper width). The structure middle width (ii) was defined as the pattern width, and the difference between it and the width of the mask pattern used was defined as the patterning error.

4. Results and Discussion

4.1 Thickness control

The measured results of the relationship between the spin-coating rotation speed and the film thickness are shown in Fig. 4. The black color shows the results of undiluted UV-PDMS and the red color shows the results of low-viscosity UV-PDMS. The measured values indicated by the dots generally fit the approximate curve shown by the dashed line. The following equation, which is a least-squares approximation of the rotation speed f and the thickness of the resist h,[16] was used to model the spin curve based on the measured values.

$$h = \frac{h_0}{\sqrt{1 + \frac{16\pi^2 f^2}{3\eta} h_0^2 t}} \tag{1}$$

Here, h_0 is the thickness of the uniform liquid layer initially applied on the horizontal surface before spinning, η is the kinematic viscosity of the liquid, and t is the rotation time, indicating that the film thickness of UV-PDMS can be controlled by adjusting the viscosity and controlling the rotational speed, as is the case with general photoresists. The range of film thicknesses that could be deposited spanned from 2 μm in the low viscosity state to 70 μm in the undiluted state. This largely covers the range of film thicknesses generally required for spin-coated MEMS structural materials.

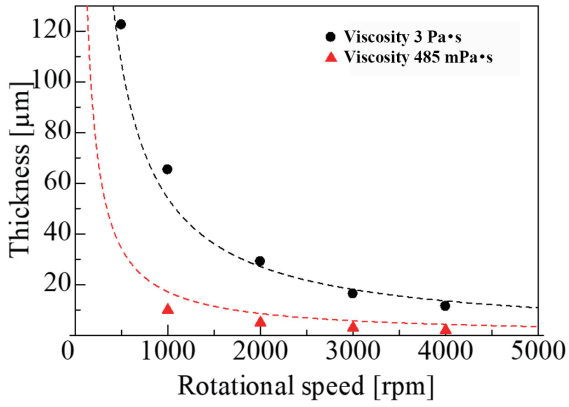

Fig. 4. (Color online) Measured spin curve of liquid UV-PDMS with varying viscosity. The dashed line is a theoretical approximation curve fitted by the least squares method using the measurement results.

4.2 Patterning accuracy

4.2.1 Exposure dose

To explore exposure parameters, exposures were made on samples with film thicknesses of 20, 30, and 40 μm. Figure 5 shows the results of a test pattern of line and space 100:100 (μm). Circles indicate the middle width of the structure, inverted triangles indicate the lower width of the structure, and triangles indicate the upper width of the structure, with the same structures connected by bars. The graph shows that the longer the bar, the greater the difference between the lower and upper widths of the structure and a trapezoidal cross-sectional shape, whereas a shorter bar represents a more rectangular pattern.

The structure middle width, which we chose as the representative dimension of the fabricated structure, showed an increasing trend at all film thicknesses past a certain minimum threshold. An ideal exposure dose around 1000–1500 mJ/cm^2 yielded a middle width that was closest to the nominal value of 100 μm for each film thickness.

The difference between the lengths of the upper and lower surfaces of the structure (bar length in Fig. 5) was 100–180 μm for all film thicknesses, and an ideal rectangular shape was not obtained at any exposure dose. Of note, patterns appear to be slightly more rectangular near the correct exposure level of 1500 mJ/cm^2. However, when the lower width of the structure was close to 200 μm, the line begins to overlap with the neighboring line pattern, potentially causing interference not representative of the actual trend. As a result, it is considered that the tendency of the pattern width with respect to the exposure dose is disturbed.

The reason for reduced rectangularity in the low exposure region is considered to be the presence of UV-PDMS in a semi-cured state at the top of the pattern due to an insufficient exposure dose. This semi-cured UV-PDMS can then flow downward and subsequently fully cure, resulting in a wider lower surface of the pattern and a narrower upper surface of the pattern. On the other hand, in the high exposure region, the width of the upper surface of the structure was close to the target value of 100 μm even when the lower surface of the structure

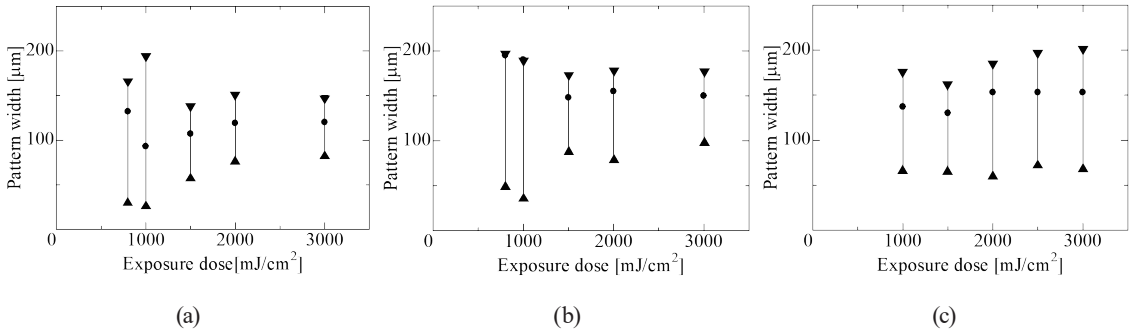

Fig. 5. Relationship between line width and exposure dose: (a) 20 μm film thickness, (b) 30 μm film thickness, and (c) 40 μm film thickness. Circles indicate the center width of the structure, inverted triangles indicate the lower width of the structure, and triangles indicate the upper width of the structure, with the same structure connected by a bar.

was close to 200 μm. Although the appropriate exposure amount was achieved on the upper surface, pattern expansion due to overexposure is likely significant on the lower surface of the structure. In other words, a nominal line width can be achieved at the top of the structure, but the sidewalls will lose verticality, resulting in a highly trapezoidal structure due to the overexposure of the bottom.

From the above results, in the range of film thicknesses for which the exposure amount was studied, a trapezoidal structure with a difference between the widths of the lower and upper surfaces of the structure of approximately 100 μm is possible at the optimum exposure amount of 1500 mJ/cm^2 and a patterning error of 30–40 μm in the middle of the resulting structure.

4.2.2 PEB

For sample preparation using PEB temperature as a variable parameter, samples with a coating thickness of 40 μm were prepared and either placed on a hot plate for 3 min at the set temperature or left at room temperature for 24 h. The SEM images in Fig. 6 show that the resulting film thickness of the sample (a) left at room temperature was 16 μm, whereas the film thickness of the sample (b) baked at 75 °C was 40 μm, which is the nominal coating thickness. The fact that the exposed area remains liquid immediately after exposure suggests that if too much time passes before curing by PEB, the exposed area will collapse and the residual film thickness after development will be reduced. As a result of pattern collapse, the pattern width is larger in (a) than in (b).

Figure 7 shows the relationship between bake temperature and patterning error as determined by image analysis. When a sample with a gap width of 100 μm was baked at more than 150 °C, the unexposed area was also cured, resulting in a complete collapse of the gap. The point with a patterning error of more than 100 μm is marked "×". The trend of the results shows that there is a minimum patterning error of about 30 μm for samples with a baking temperature of 75 °C. If the temperature is very low, the above-mentioned collapse occurs and the patterning error increases. On the other hand, if the temperature is very high, unexposed areas undergo partial thermal curing, also increasing the error.

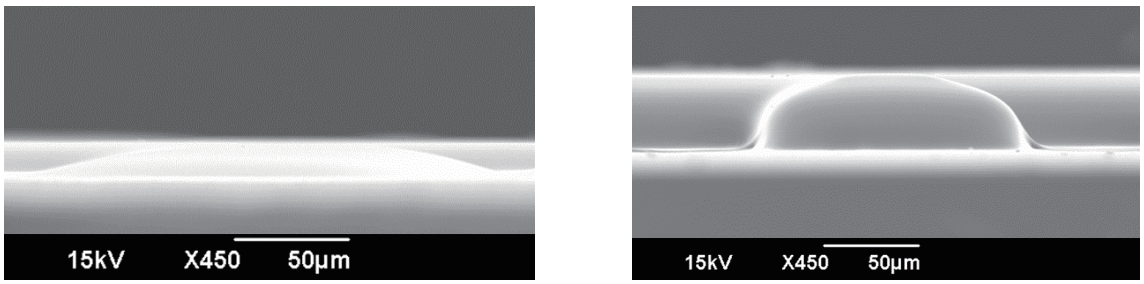

(a) (b)

Fig. 6. Cross-sectional SEM images of the line pattern with a nominal thickness of 50 μm. (a) Structure with no PEB left at room temperature for 24 h. (b) Structure baked at 100 °C for 3 min. The microstructures were exposed from the bottom of the image.

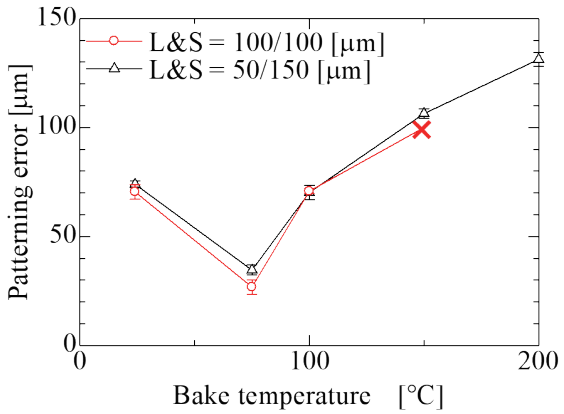

Fig. 7. (Color online) Patterning error versus bake temperature after exposure.

4.2.3 Development using organic solvent

To evaluate the effects of different developer solvents on the dissolution of the uncured area after PEB, a sample with a layer thickness of 30 μm was used to develop the film with a development time of 5 min. Figure 8 shows the SEM images of the line shapes observed after development and Fig. 9 shows the relationship between the patterning error measured from the images and the SP value of the solvent. The figure shows that the smallest patterning error was observed for hexane with an SP value of 7.3. The closer the SP values of the solute and solvent are, the easier it is to dissolve, and the SP value of hexane is closest to that of UV-PDMS of 7.4. The higher solubility of UV-PDMS in hexane than in other solvents resulted in less residue, and the faster dissolving efficiency meant that less swelling was required to develop the uncured UV-PDMS.

4.2.4 Optimization of photolithography conditions

On the basis of the results of the patterning accuracy experiments performed, the optimum fabrication parameters for processing UV-PDMS by photolithography are as follows. In the film thickness range from 20 to 40 μm, the appropriate exposure dose is 1000–1500 mJ/cm^2, PEB should be performed at 75 °C for 3 min, and a hexane-based solvent is appropriate for development. These conditions should reduce the patterning error to about 30 μm.

Although the patterning error is higher than that of conventional photoresists, it is possible to fabricate MEMS devices whose feature size exceeds the patterning error. Moreover, as mentioned in Sect. 4.2.1, one of the reasons for the large patterning error and slope on the exposed sidewall is considered to be the significant variation (attenuation) in exposure dose across the thickness of UV-PDMS. Therefore, the exposure of UV-PDMS using 3D lithography[5,17,18] is expected. 3D lithography is a method of adjusting the exposure dose distribution in the film by controlling the direction of the UV light entering the photoresist. We will investigate an exposure method to improve patterning accuracy by adjusting the distribution of exposure dose within UV-PDMS using 3D lithography as a future work.

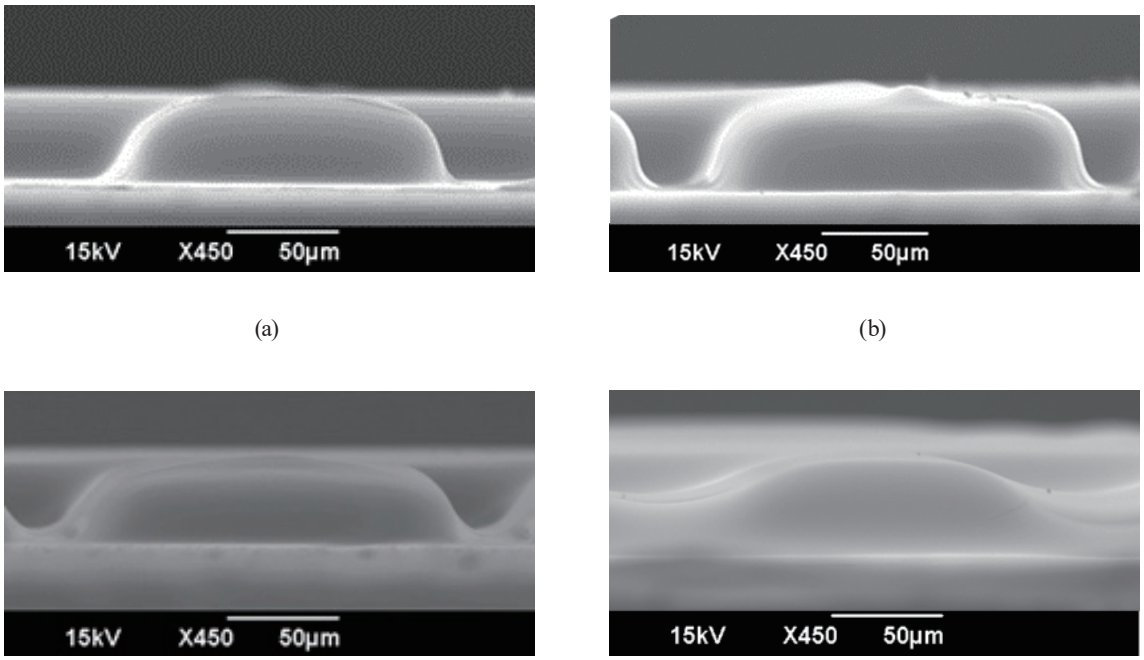

Fig. 8. Cross-sectional SEM images of the line patterns dissolved in various solvents: (a) hexane, (b) toluene, (c) tetrahydrofuran, and (d) acetone. The microstructures were exposed from the bottom of the image.

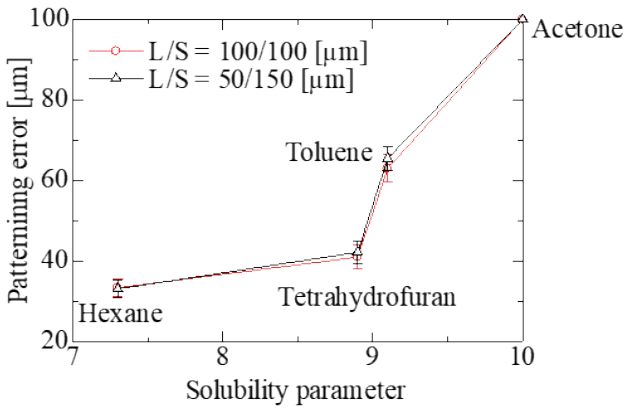

Fig. 9. (Color online) Relationship between the SP value of the solvent used for development and the patterning error. Structures developed in acetone are marked "×" at a patterning error of 100 µm, as no clear independent structure was observable.

Additionally, UV-PDMS enables some geometries difficult to achieve otherwise. In the proposed method, only the exposed area remains, such that free-standing PDMS thin films with microstructures, including through-structures, can be obtained on a wafer-size exposure area.

5. Application for MMs Made of UV-PDMS

5.1 MMs

Metamaterials have been actively studied in the field of electromagnetics as materials with negative dielectric constant and magnetic permeability.[19,20] By incorporating artificially created microperiodic structures, materials and structures with properties not found in natural materials are now being investigated for a wide range of material properties.[21] MMs, which are characterized by their unique mechanical properties, are also being studied, from structural investigations of MMs with a negative Poisson's ratio[22] to applications such as vibratory energy-harvesting devices using MMs.[23]

Owing to its excellent elasticity and flexibility, UV-PDMS has a very high affinity for metamaterial structures with a negative Poisson's ratio. In this study, MMs consisting of typical cellular structures in the form of 2D re-entrant hexagonal honeycombs were designed, as shown in Fig. 10. MMs were tested in uniaxial tensile tests. Similar samples of SU-8 3050 (Nippon Kayaku) thick-film photoresist for permanent structures were also prepared using the same mask pattern and the material properties were compared.

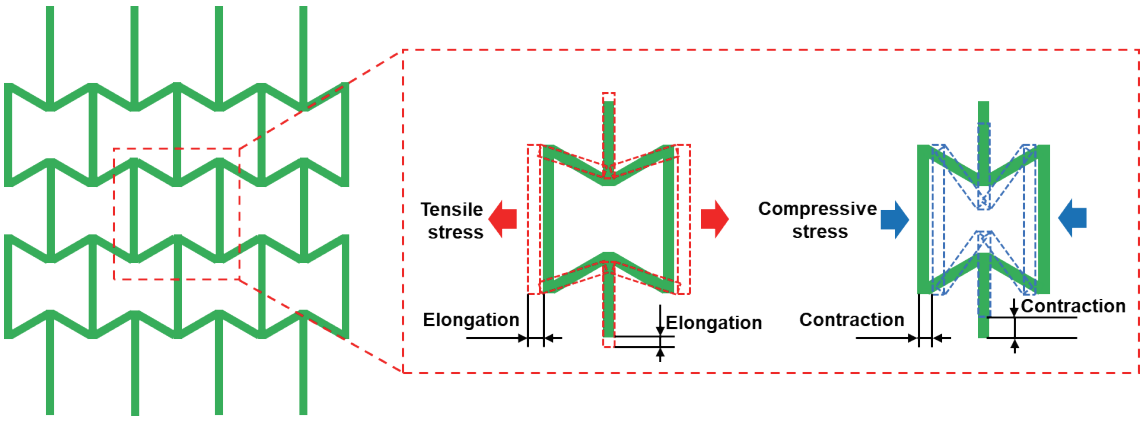

(a)

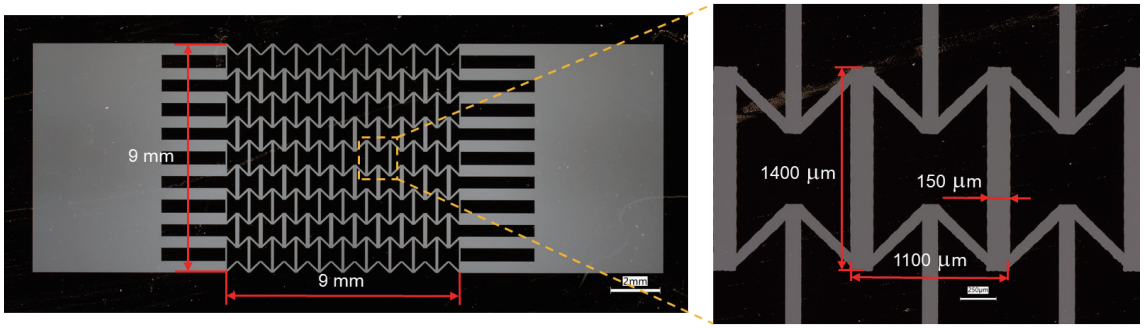

(b)

Fig. 10. (Color online) MM having negative Poisson's ratio. (a) Schematic mechanism of MM. (b) Photograph of mask pattern of MM specimen for tensile test.

5.2 Design and fabrication of MM specimens

An MM specimen (MMS) for uniaxial tensile testing with the geometry shown in Fig. 10(b) was fabricated under optimized processing conditions for a design film thickness of 80 μm. Two photomasks were used: a normal mask with nominal pattern dimensions and a corrected mask with pattern dimensions that account for patterning errors discussed in the previous section. Magnified images of the normal mask and SEM images of the UV-PDMS structure fabricated using it are shown in Figs. 11(a) and 11(b), respectively. The figure shows that the pattern width of the links in the fabricated structure is large, and the links collapse owing to the overlap of the pattern spread as well as optical proximity effects. On the other hand, magnified images of the corrected mask and SEM images of the UV-PDMS structure fabricated using the mask are shown in Figs. 11(c) and 11(d), respectively. Furthermore, by using a corrected mask with a step at the junctions where the pattern was notably thickened, a structure with a patterning error of less than 5% of the target line width was produced. The SU-8 MMS for comparison was fabricated using the normal mask shown in Fig. 11(a) by combining photolithography and a sacrificial layer release process.

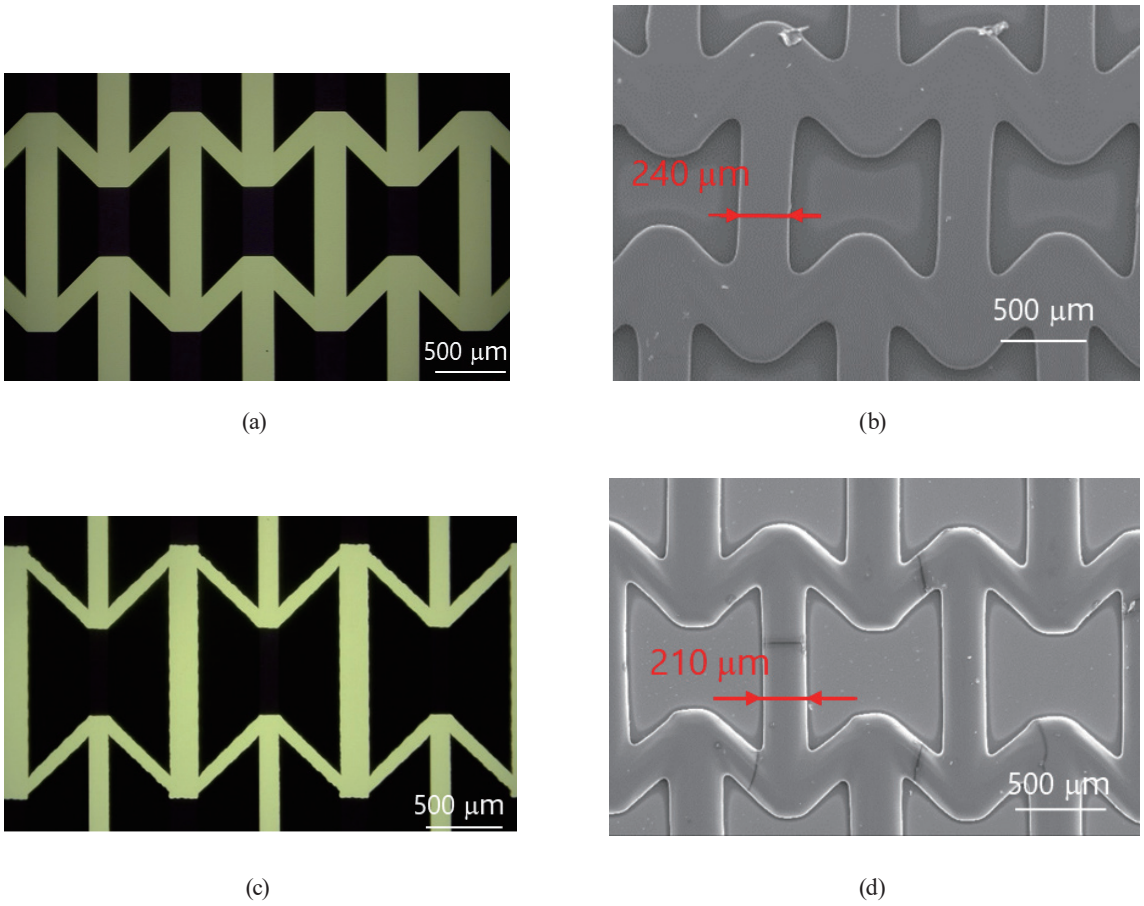

(a) (b)

(c) (d)

Fig. 11. (Color online) Photographs of the mask pattern and SEM images of resulting MMS: (a) normal mask, (b) MMS produced with normal mask, (c) corrected mask, and (d) MMS produced with corrected mask.

5.3 Tensile test of MMS

Figure 12(a) shows a photograph of an MMS in a uniaxial tensile test. One end of the MMS handle was fixed and the other end was attached to a movable precision table, which was used to deform the MMS. The behavior of the MMS during the tensile test was observed from above using a digital microscope (VHX-1000, Keyence Corp.). Images were taken for the movement of the precision stage in the longitudinal direction of the MMS, and the contour of the metamaterial feature was measured. The effective Poisson's ratio of the structure is defined as the ratio of the strains calculated from the elongation of the whole MMS outline in the longitudinal and transverse directions of the MMS and is expressed as

$$\upsilon = -\frac{\varepsilon'}{\varepsilon}. \tag{2}$$

Here, ε' is the transverse strain and ε is the longitudinal strain. The appearance of the MMS during the tensile test is shown in Figs. 12(b) and 12(c), where Fig. 12(b) shows the MMS before the tensile load is applied and Fig. 12(c) shows the most elongated state of the MMS in the direction perpendicular to the tension. The figure shows that the MMS contour does not shrink in the transverse direction; in other words, the negative Poisson's ratio effect of the MM is apparent.

Figure 13 shows the biaxial elongation from the tensile test. Focusing on the elongation in the tensile direction, the maximum elongation of the UV-PDMS MMS is 230%, which is about 12 times higher in the tensile direction than that of the SU-8 MMS. A larger amount of deformation was obtained by using UV-PDMS and the proposed method to fabricate a through-structure,

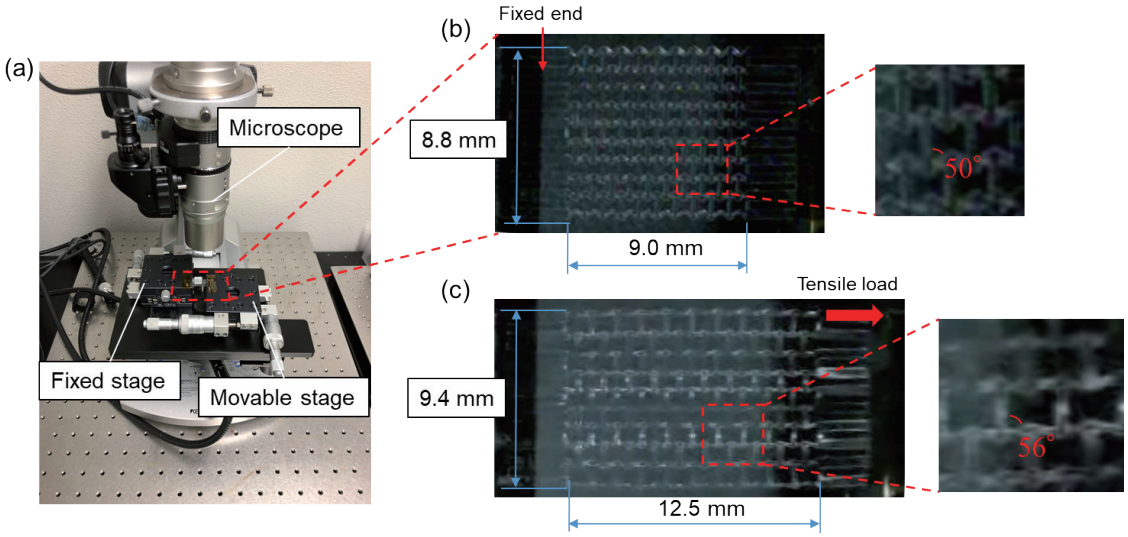

Fig. 12. (Color online) Experimental setup for uniaxial tensile test. (a) Direct observation of the sample under an optical microscope. (b) View of the specimen before stretching. (c) View of the specimen when the precision stage is moved 3 mm.

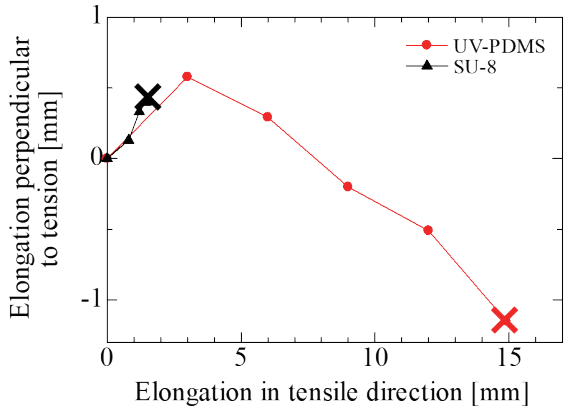

Fig. 13. (Color online) Relationship between biaxial strains in uniaxial tensile tests.

which was difficult to fabricate with the conventional thermally cured PDMS. Next, when the Poisson's ratio for each measurement point was calculated, the Poisson's ratios calculated at the point of maximum transverse strain are −1.05 for the SU-8 MMS and −1.30 for the UV-PDMS MMS, with the UV-PDMS MMS having a higher negative Poisson's ratio. Although the negative Poisson's ratio was not obtained in the entire tensile region, it was found that the negative Poisson's ratio was maintained up to a tensile region about four times wider than that of the conventional SU-8 MMS. For the MMs with a negative Poisson's ratio used in this study, the use of UV-PDMS allowed the fabrication of MMs with a higher performance than the case of using SU-8. The above results show promise for the application of UV-PDMS to MMs in general and specifically to MEMS incorporating MMs. Since the mechanical strength of MMs with microstructures is lower than that of solid structures, the mechanical durability of the proposed UV-PDMS should be considered for practical application as a mechanical deformation device. The relationship between periodic structure size and structural strength using the general photoresist are mentioned in Ref. 23.

6. Conclusions

In this study, a patterning method using photolithography was proposed as a microfabrication method for UV-PDMS. It was found that UV-PSDMS can be controllably deposited and patterned at thicknesses comparable to those of conventional thick-film resists. In addition, free-standing flexible thin films with microstructures, including through-structures, were obtained on a wafer-size exposure area. Optimal processing conditions were investigated, and patterning errors were suppressed to about 30 μm. Furthermore, UV-PDMS metamaterial samples were fabricated as an example for potential soft MEMS applications. Tensile test results showed that the use of UV-PDMS produced metamaterials with a higher deformation than the case of using SU-8. These results indicate that UV-PDMS can be processed by photolithography and is expected to be applied to various devices by exploiting its excellent physical properties.

Acknowledgments

This work was supported in part by JST CREST JPMJCR19Q2, JSPS Grants-in-Aid for Scientific Research JP20H02095, JP20K20626, and JP22H02105, and Gunma University Priority Support Projects G3.

References

1 J. Yunas, B. Mulyanti, I. Hamidah, M. M. Said, R. E. Pawinant, W. A. F. W. Ali, A. Subandi, A. A. Hamzah, R. Latif, and B. Y. Majlis: Polymers **12** (2020) 1184. https://doi.org/10.3390/polym12051184
2 C. Liu: Adv. Mater. **22** (2007) 3783. https://doi.org/10.1002/adma.200701709
3 C. H. Lin, G. B. Lee, B. W. Chang, and G. L. Chang: J. Michromech. Microeng. **12** (2002) 591. https://doi.org/10.1088/0960-1317/12/5/312
4 B. J. Kim and E. Meng: J. Micromech. Microeng. **26** (2016) 013001. https://doi.org/10.1088/0960-1317/26/1/013001
5 T. Iida, T. Tsukamoto, K. Miwa, S. Ono, and T. Suzuki: Sens. Mater. **31** (2019) 2527. https://doi.org/10.18494/SAM.2019.2309
6 H. Nishida: Polym. J. **43** (2011) 435. https://doi.org/10.1038/pj.2011.16
7 H. Ueno, K. Maruo, M. Inoue, H. Kotera, and T. Suzuki: Micromachines **11** (2020) 571. https://doi.org/10.3390/mi11060571
8 T. Tamai, K. Maruo, H. ueno, K. Terao, H. Kotera, and T. Suzuki: Biomicrofluidics **9** (2015) 022405. https://doi.org/10.1063/1.4917511
9 M. Shirai and H. Okumura: Polym. Int. **65** (2016) 362. https://doi.org/10.1002/pi.5065
10 J. Kim, H. An, Y. Seo, Y. Jung, J. S. Lee, N. Choi, and K.W. Bong: Biomicrofluidics **11** (2017) 024120. https://doi.org/10.1063/1.4982698
11 K. Obata, S. Slobin, A. Schonewille. A. Hohnholz, C. Unger, and J. Koch: Appl. Phys. A **495** (2017) 2. https://doi.org/10.1007/s00339-017-1104-1
12 D. Troegel and J. Stohrer: Coord. Chem. Rev. **255** (2011) 1440. https://doi.org/10.1016/j.ccr.2010.12.025
13 J. B. Lee, K. Choi, and K. Yoo: Micromachines **6** (2015) 1. https://doi.org/10.3390/mi6010001
14 I. Song, K. Kang, Y. Jin, D. Park, and P. K. Ajmera: Microsyst. Technol. **14** (2008) 1285. https://doi.org/10.1007/s00542-007-0510-2
15 K. Kim, D. S. Park, H. M. Lu, W. Che, K. Kim, J. B. Lee, and C. H. Ahn: J. Micromech. Microeng. **14** (2004) 597. https://doi.org/10.1088/0960-1317/14/4/021
16 H. J. Levinson: Principles of Lithography (SPIE Press, USA, 2005) 2nd ed., p. 63.
17 T. Suzuki, H. Kotera, I. Kanno, and D. Hiramaru: U.S. Patent 8871433 (2014).
18 T. Tsukamoto, Y. Umino, S. Shiomi, K. Yamada, and T. Suzuki: Sci. Technol. Adv. Mater. **19** (2018) 660. https://doi.org/10.1080/14686996.2018.1508985
19 K. Masuda, S. Ogawa, Y. Takagawa, and M. Kimata: Sens. Mater. **26** (2014) 215. https://doi.org/10.18494/SAM.2014.972
20 A. Yu, W. Li, Y. Wang, and T. Li: Sens. Mater. **30** (2018) 2719. https://doi.org/10.18494/SAM.2018.2001
21 N. Novac, M. Vesenjak, and Z. Ren: J. Mech. Eng. **62** (2016) 485. https://doi.org/10.5545/sv-jme.2016.3656
22 T. Beckmann, N. Stenger, M. Kadic, J. Kaschke, A. Frolich, T. Kennerknecht, C. Eberl, M. Thiel, and M. Wegener: Adv. Mater. **24** (2012) 2710. https://doi.org/10.1002/adma.201200584
23 R. Ichige, N. Kuriyama, Y. Umino, T. Tsukamoto, and T. Suzuki: Sens. Actuator, A **318** (2021) 112488. https://doi.org/10.1016/j.sna.2020.112488

About the Authors

Ten Sekiguchi received his B.S. degree from Gunma University, Japan, in 2021. He is pursuing his M.S. degree in the Division of Mechanical Science and Technology at the same university. His research interests are in MEMS and related microfabrication technologies. (t211b049@gunma-u.ac.jp)

Hidetaka Ueno received his B.S. and M.S. degrees from Kagawa University, Japan, in 2014 and 2016, respectively. He received his Ph.D. degree from Gunma University, Japan, in 2019. From 2019 to 2020, he was a postdoctoral researcher at Gunma University. From 2020 to 2023, he was a postdoctoral researcher at the National Institute of Advanced Industrial Science and Technology. Since 2023, he has been a project assistant professor at Kobe University. His research field is bioengineering. (hueno@people.kobe-u.ac.jp)

Vivek Anand Menon received his B.S. degree from the University of California, Berkeley, U.S.A., in 2013, and his M.S. and Ph.D. degrees from The University of Tokyo, Japan, in 2016 and 2021, respectively. He is currently a project researcher at The University of Tokyo. His research interests include liquid cell transmission electron microscopy (LCTEM) and optical MEMS. (vmenon@iis.u-tokyo.ac.jp)

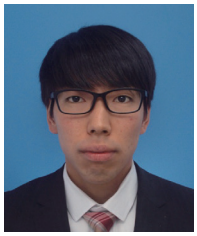

Ryo Ichige received his B.S. and M.S. degrees from Gunma University, Japan, in 2019 and 2021, respectively. His research interests are in MEMS and energy harvesting for IoT. (t191b009@gunma-u.ac.jp)

Yuya Tanaka received his B.S. degree in electrical engineering from Chiba University in 2008, and his M.S. and Ph.D. degrees from the Graduate School of Advanced Integration Science, Chiba University, in 2010 and 2013, respectively. He worked in the OLED R&D Department of Japan Display Inc. for three years. From 2016 to 2022, he was an assistant professor at the Center for Frontier Science, Chiba University. He also worked as a PRESTO researcher of the Japan Science and Technology Agency (2017–2021). Since 2022, he has been an associate professor at the Graduate School of Science and Technology, Gunma University. His research interests include the behavior of charge carriers in organic semiconductor devices and the development of electret-based devices composed of polar organic molecules, such as vibrational energy harvesters. (yuya.tanaka@gunma-u.ac.jp)

Hiroshi Toshiyoshi received his M.E. and Ph.D. degrees in electrical engineering from The University of Tokyo, Tokyo, Japan, in 1993 and 1996, respectively. He joined the Institute of Industrial Science (IIS), The University of Tokyo, in 1996 as a lecturer. From 1999 to 2001, he was a visiting assistant professor at the University of California, Los Angeles, CA, U.S.A. In 2002, he became an associate professor with the IIS, The University of Tokyo. From 2005 to 2008, he was the project leader of the Optomechatronics Project at the Kanagawa Academy of Science and Technology, Kawasaki, Japan. Since 2009, he has been a professor with the IIS, The University of Tokyo. His research interests include optical and power MEMS. (hiro@iis.u-tokyo.ac.jp)

Takaaki Suzuki received his B.E. and M.E. degrees from Gunma University, Japan, in 1998 and 2000, respectively. He also received his Ph.D. degree from Kyoto University, Japan, in 2003. From 2004 to 2008, he was an assistant professor at Kyoto University. From 2008 to 2015, he was an associate professor at Kagawa University. From 2015 to 2018, he was an associate professor at Gunma University. Since 2018, he has been a professor at the Division of Mechanical Science & Technology, Gunma University. From 2015 to 2019, he was also a PRESTO researcher at the Japan Science and Technology Agency. His research interests include the development of novel microfabrication technology, microfluidic systems for gene and cell analyses, and an energy harvester for IoT. He is a member of IEEE, the Japan Society of Mechanical Engineers, the Institute of Electrical Engineers of Japan, and so forth. (suzuki.taka@gunma-u.ac.jp)